Composites Part B: Engineering 243 (2022) 110123
10.1016/j.compositesb.2022.110123

Tensile failure strain and microstructure of unidirectional carbon fibre non-crimp fabric composites

Francisco Mesquita[1], Arsen Melnikov[1], Ashok Rajpurohit[2], Vicky Singery[2], Phillipe Sanial[2], Stepan V. Lomov[1], Yentl Swolfs[1*]

[1]Department of Materials Engineering, KU Leuven, Kasteelpark Arenberg 44 box 2450, 3001 Leuven, Belgium

[2]Chomarat Textiles Industries, 39 Avenue de chabannes, 07160 Le Cheylard, France

[*]Corresponding author: yentl.swolfs@kuleuven.be, +3216373616

Abstract

UD non-crimp fabric (NCF) carbon/epoxy composites were tested in longitudinal tension to assess the influence of the stitching on the tensile failure strain of the carbon fibre layers. The composites made with the stitched layers had the same tensile failure strain as the reference non-stitched layer composite. A composite where the stitching yarns has been removed appears to have a lower failure strain though. Computed tomography images revealed that the regions adjacent to the stitch showed the highest fibre volume fraction. The stitched layers clearly showed a higher fibre misalignment than the non-stitched layers. The fibre misalignment was very low in the layers in which the stitches were removed. The observations suggest that the fibre distortions due to stitching do not reduce the failure strain; the distortions caused by removing the stitches are detrimental and reduce the failure strain.

Keywords: A. Polymer-matrix composites (PMCs); B. Mechanical properties; B. Microstructures; E. Stitching; Non-crimp fabrics

1 Introduction

The fibres in a composite material are the main load carriers and are often oriented towards the main loading direction to optimise the stiffness and strength. Even in multidirectional composites, where the tensile failure is influenced by off-axis cracks and delamination, the final failure is controlled by fibre break development [1]. Understanding the factors that influence the longitudinal tensile strength of unidirectional composites is of high importance to understand the tensile failure of any composite material.

The products used to manufacture thermoset composite materials are either pre-impregnated fibre layers that can be stacked together and cured or dry fibre layers that are stacked and then impregnated and cured. In the dry case, the binding of the fibres within a layer can be made through binders or through stitching. Resin channels or local distortion of the fibres can be created depending on the stitching pattern. Apart from non-structural stitching to ease the fabric handling, the fibrous layers can be reinforced in the thickness direction with so-called structural stitching, which creates a 3D reinforcement structure and affects delamination resistance and through-the-thickness mechanical properties [2-4]. In the present work, only non-structural stitching is considered.

Although structural stitching is beneficial for the through-the-thickness properties, it has been found to degrade the in-plane properties such as tension, compression, and shear [2-

4]. For non-structural stitching used in non-crimp fabrics (NCFs), the results are ambiguous. The in-plane tensile modulus has been found to not be influenced by the stitching [5]. Several authors have also shown that non-structural stitching degrades the tensile properties of composites [5-15]. Rimmel et al. [6] observed that the tensile failure of UD carbon fibre non-crimp fabric (NCF) composites initiated at the stitching point. The same was established for multiaxial NCFs [5,16]. Kang and Lee [8] showed a consistent decrease of the tensile modulus and strength of an S-2 glass/polyester composite when the spacing between stitches decreases but it is unclear how the failure strain evolves. Failure strain is a better parameter for this type of comparisons, as it is almost unaffected by fibre volume fraction changes [17,18] due to stitching. An increased linear density of the stitching yarn also appears to reduce the tensile strength of carbon fibre composites [9-11]. It should be noted that these studies did not guarantee a proper tensile failure in the gauge section, thus making the results presented ambiguous.

The stitching of the composite has been shown to damage only 0.5% of all the fibres [19], so it is unlikely that fibre damage influences the tensile strength. The most likely mechanism is the local fibre orientation. A 5º global misorientation has been shown to decrease the tensile failure strain by 20% but a larger angle actually increased the failure strain [20].

Some researchers have measured the degree of fibre misalignment through optical microscopy around a structural stitch in unidirectional composites showing an in-planemisalignment angle of up to 8.5º [21]. The maximum in-plane misalignment angle depended on the diameter of Z-pins, being 4º and 5.4º when the Z-pin diameter was 0.28 mm and 0.51 mm, respectively [22]. Rouf et al. [23] reported the maximum in-plane and out-of-plane misalignment angles to be 19° and 5°, respectively, in a stitched UD NCF. Gonzalez et al. [24] predicted the in-plane tensile stiffness to reduce roughly linear with the out-of-plane angle. In all these cases, however, the angles were measured at the mesoscale, without considering individual fibre alignment.

Other authors have also used the geometry of the resin-rich region to model the fibre volume fraction and in-plane misalignment angle distribution surrounding it in UD [25-27] and multiaxial [28] NCFs. These models were conceptualised based on an idealised shape of the stitching distortion. The assumptions should therefore be verified through experimental observations of the real shape.

This paper analyses the tensile failure strain of several warp-knitted NCF unidirectional carbon fibre reinforced composites by sandwiching the stitched layers between S-glass layers and thus removing the effect of the stress concentrations imposed by the grips [29]. The composites were then scanned with X-ray computed tomography to determine the distribution of fibre volume fraction and misalignment angle surrounding the stitch. The goal was to correlate changes in the tensile failure strain with the fibre microstructure in the composite. Apart from UD laminates made of the warp-knitted and unstitched layers, composites reinforced with UD NCF plies with the stitching manually removed were also studied.

2 Materials and methods

2.1 Materials

The goal of this study was to assess the tensile failure strain of stitched carbon fabrics with different production parameters. Carbon fibre rovings containing T700SC-12K-50C

fibres (Toray Industries, Japan) were spread by Chomarat (France) to create a unidirectional tape with an areal density of 106 g/m^2. The unidirectional stitched fabrics were then manufactured using the spread tape and polyester (PES) stitching yarns forming a 45º angle with the fibre direction (see Figure 1a). The pitch length and gauge were 3.25 mm and 4.9 mm, respectively, and a chain warp-knitting pattern was used for all the fabrics. The stitching yarn linear density and yarn tension were varied to understand their influence on the tensile failure strain of the carbon fibres and fibre microstructure.

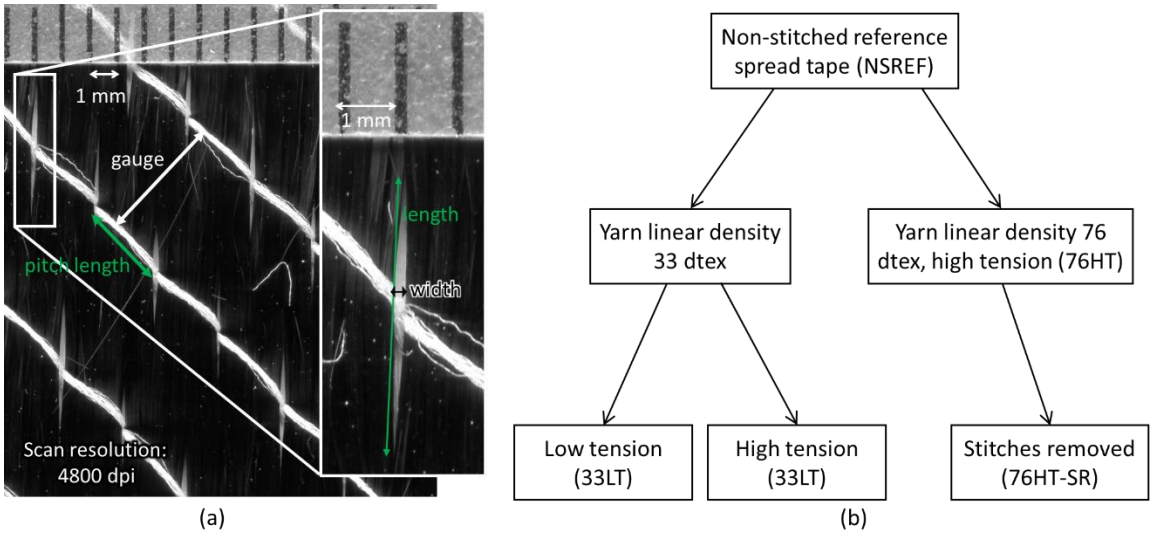

***Figure 1** – Carbon fibre fabric: (a) dry fabric image showing the 45º orientation of the stitching yarn and (b) production parameters schematics.*

Five types of carbon fabrics were produced for this study. The first one consisted of the unidirectional spread tape without stitching and served as a reference (NSREF). The other fabrics were stitched using a PES yarn with a linear density of either 33 or 76 dtex. Different yarn tension was applied to the fabrics stitched with a 33 dtex linear density yarn. The high tension (33HT) corresponds to 4.7 m/rack and the low tension (33LT) corresponds to 5.1 m/rack. The fabric with the 76 dtex linear density yarn (76HT) was stitched using high tension. The yarn tension is inversely related to the value of the stitching yarn supply per length of the fabric, which is expressed in meters per rack. A rack corresponded to 480 piercing points. Using a shorter length of yarn over one rack leads to a significantly higher tension in the stitching yarn. The fifth fabric (76HT-SR) was produced by removing the stitching yarn manually from some of the 76HT fabric. The goal was to understand whether the removal of the stitching yarn would lead to a recovery of the fibre alignment and influence the tensile failure strain. The 76HT fabric was chosen for this sub-study because its stitching parameters were expected to produce the largest changes in the fibre microstructure. Figure 1b shows a schematic of the fabric production parameters.

The continuous tab approach of Czél et al. [29] was used to prevent preferential fracture of the tensile specimens at the grips. The carbon fabrics were therefore sandwiched between unidirectional S-glass layers (supplied by LBIE) with an areal density of 173 g/m^2. The stacking sequence of all specimens was ($SG_3/C_2/SG_3$) where “SG” and “C” refer to the S-glass and carbon fabrics, respectively and the sub-indices refer to the number of layers of such type. Following the study of Wisnom et al. [30], the number of carbon layers was set to 2 so that a potential hybrid effect was ruled out in the

interpretation of the results. The thermal residual strain effect of combining different fibre types in the same composite will be accounted for in the calculation of the failure strain (see section 2.2.3). The dry fabrics were impregnated with a two-phase epoxy resin consisting of the Epikote 828 resin (Hexion, USA) and hardener DCH 99 (Dytek, USA) with a ratio of 15,2g of hardener per 100g of resin.

2.2 Methods

2.2.1 Resin transfer moulding

All the composites were manufactured using resin transfer moulding (RTM). The fabrics were cut into layers of 450x450 mm and stacked according to the stacking sequence described in section 2.1. A 1 mm thick spacer was used, as this led to a reasonable V_f. The fabrics were then placed in the RTM mould together with the spacer and closed with a pressure of 200 bar. The resin was mixed and placed in a vacuum chamber for 15 min to remove entrapped gases and thus decrease the void content of the composite.

Vacuum was then applied to the resin outlet of the mould while it was kept at a temperature of 43 ºC. The resin was injected with an overpressure of 1 bar until resin was seen at the outlet of the mould. At this point, the overpressure was increased to 4 bar to compress the potential air pockets in the composite and kept for 2 min. The temperature of the mould was then increased to 75 ºC and maintained for 90 min. After the curing time, the mould was cooled down and the composite panel removed. The composite panel was then placed in an oven for 2h at 150 ºC to achieve full curing of the resin. The resulting thickness of all the panels was 1.15±0.04 mm. Based on the methodology described in section 2.2.5, we calculated a global fibre volume fraction of 45.5±1.6%.

2.2.2 Specimen preparation

The specimens measured 15 mm in width and 250 mm in length and were cut from the composite panel using a diamond-coated rotating saw. The specimen's longitudinal edges were parallel to the fibre direction. After cutting, 4 mm thick end-tabs made of woven E-glass/epoxy were bonded to the specimens. The end tabs were 50 mm in length and approximately 20 mm in width. The end-tabs were slightly wider than the specimens to ensure the end-tabs fully cover the specimen ends. The end-tabs were bonded using 3M Scotch-Weld EC 9323 B/A. The adhesive was cured at 100ºC for 15 min. A speckle pattern was applied to the surface of the specimen to enable the strain measurement using digital image correlation.

2.2.3 Tensile testing

Tensile tests were performed according to ASTM D3039 [31] using a Zwick Z100 universal testing machine equipped with a 100 kN load cell. The gauge length was 150 mm, and the displacement rate was 1 mm/min. 10-11 specimens were tested for each configuration (see Table 1). Half of the specimen width was speckled with a fine marker. The images used for the digital image correlation were captured using a Limess Vic3D camera, and the regions near the grips were avoided in the correlation. The strain was measured using digital image correlation through the software package VIC2D from Correlated Solutions. The subset and step sizes were 17 and 5 pixels, respectively. The pixel size was approximately 0.1 mm.

After processing the tensile test results, the strain values were corrected to take into account the thermal residual strains due to the combination of carbon and glass fibres in

the same composite. Considering that the fibres would contract differently from the curing temperature to room temperature if they were not bonded together, the theoretical strain difference for each fibre type can be calculated. Given that the fibres were in fact bonded together, an equilibrium can be established based on equation 1.

$$\varepsilon_{eq\,c}=\left(\varepsilon_{fr\,g}-\varepsilon_{fr\,c}\right)-\frac{t_c\cdot E_c\left(\varepsilon_{fr\,g}-\varepsilon_{fr\,c}\right)}{t_c\cdot E_c+t_g\cdot E_g} \quad (1)$$

Where ε_{eq} is the equivalent strain in the respective layer, the subscripts *g* and *c* correspond to the glass and carbon layers, respectively, ε_{fr} corresponds to the free strain, given by the product of the coefficient of thermal expansion and the temperature, divided by the initial length of the layer, *t* corresponds to the layer thickness and *E* corresponds to the layer longitudinal stiffness.

2.2.4 Micro-computed tomography

A TeScan UniTOM HR X-ray micro-computed tomography (CT) scanner was used to acquire volumetric images of the stitched layers to characterise their microstructure. The stitched carbon layers were separated from the S-glass after the tensile tests were performed. During the tensile tests, the carbon layers fractured and delaminated, easing their separation from the S-glass layers. The width of the CT specimens was 2.5±0.2 mm to enable a small voxel size while maintaining a high probability of having a stitching point region in the scan.

The CT scan was performed with the following acquisition parameters: electric potential was 60 kV, the power was 1 W, the number of projections was 4353 with 3 images taken per projection, the exposure time was 1.25s, the voxel size was 0.99 μm and the nanofocus mode was used. The detector had 2916x2280 pixels, which leads to an image size of 2.88 m x 2.26 mm. The nanofocus mode decreases the spot size of the X-ray emission but a low power needs to be used, thus increasing the scan time.

2.2.5 Microstructural characterisation

The CT scans were obtained to characterise the fibre microstructure in the vicinity of a stitching point, which is where we expect to find fibre misalignment and volume fraction variation. The obtained images (see Fig. 2) provide a large data set which cannot be analysed manually. The InSegt algorithm [32,33] was used to segment the fibres in the scans. InSegt uses a machine learning approach where the user trains the algorithm to identify fibre centres in a subset (100x100 μm) of the original images of the longitudinal cross-section. The algorithm then proceeds to identify the fibre centres in the remainder of the images. The fibre centres are used to track fibre trajectories using a nearest neighbour search. Not all the cross-sectional slices were used to identify the fibre centres because a large computational time would be necessary, and the fibre tracking would not be improved. Cross-sectional slices in steps of 10 μm were used to track the fibre centres. The fibre trajectories can be used to determine the fibre misalignment angle. The local fibre misalignment angle is computed for 100 μm long fibre segments, which we found long enough to minimise noise while still short enough to capture accurately the local fibre alignment. For more information about the InSegt algorithm, the reader is referred to [32,33].

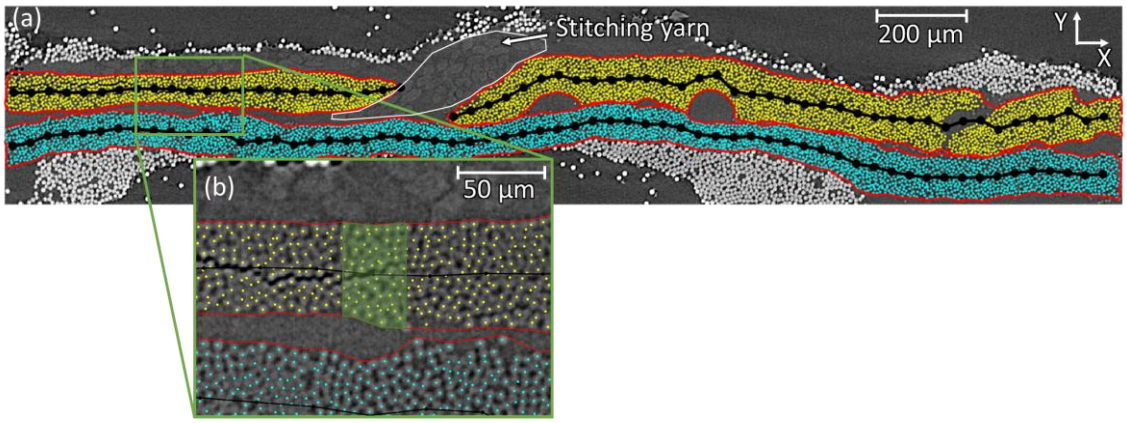

***Figure 2** – Computed tomography images used for the analysis of fibre volume fraction and misalignment angle. The yellow and cyan points in (a) correspond to the fibre centres detected in layers 1 and 2, respectively, the red lines define the boundaries of the layers and the black lines with the circles define the midline of each layer. The green shaded region in (b) corresponds to a region where the fibre volume fraction or misalignment angle are calculated.*

The InSegt algorithm was not able to identify all the fibre centres in a cross-sectional slice. Performing the training step 3 times in different image subsets instead of once increased the relative number of the identified fibre centres from a maximum of 73% to 80%. The fraction of fibre centres identified was obtained by comparison with 10 slices where all the fibre centres were identified manually. These 10 slices were used to calculate the distribution of fibre volume fraction, v_f, in the 33LT and 76HT specimens. The local fibre angle, θ, was obtained using the fibre trajectories identified by InSegt where only the 80% of the fibre centres were available.

The information on the fibre centre locations and local angle are obtained in the 3D coordinates of the volume. However, the stitching point is expected to produce variation of these properties in the direction of the fibre length (Z) and width of the layers (X). The variation of v_f and θ in the thickness direction is not expected to be affected by the stitch and will be assumed to be negligible in the analysis. To obtain the variation of v_f and θ in the X and Z direction, the values were averaged through the thickness. The first step was to associate each fibre centre to its corresponding layer in the composite (see Figure 2). The fibre centres were then used to define the boundaries of each layer region using the MATLAB function "boundary". It is important to define the area of each layer region to accurately obtain the fibre volume fraction inside of each bundle.

For each layer, the width direction was divided into evenly spaced sections with a width of 40 microns. For each layer, v_f and θ can then be calculated as a function of X for each cross-sectional slice. For v_f, the number of fibre centres in each section of the layer (see Figure 2) was obtained and divided by the area of the section (40 microns x local thickness of the layer). For θ, the local angle of the fibres inside a section was averaged. The local angle was obtained in plane, θ_{IP} (XZ) and out of plane, θ_{OP} (YZ). By performing these steps for all the cross-sectional slices in the Z direction, the distribution of v_f and θ can be obtained in the X and Z direction. A smoothing surface was then fitted to the data points in the X and Z direction using the "lowess fit" function of MATLAB with a span of 0.15 to provide a distribution of v_f and θ over the entire space. The span parameter defines the region over which the fitting is performed where 1 corresponds to the entire

space. The standard deviation of the smoothing surface fit was 2% for v_f and 0.4º for the local angle.

3 Results and discussion

3.1 Failure strain

The tensile tests provide information on the failure strain, strength, and stiffness of the composites. As the methodology used in this study involved the use of hybrid composites to prevent preferential fracture near the grips, the stiffness and strength values obtained were for the hybrid and not for the stitched carbon fibre layers. Figure 3 therefore compares the failure strain of the different types of the manufactured composites.

The p-values were computed for all pairs of fabrics to determine whether their failure strain differences were statistically significant. Comparing all the stitched fabrics with the reference case NSREF (see Table 1), it was found that only the 76HTSR was significantly different with a p-value of 0.1%. All the other stitched fabrics had a p-value higher than 5% relative to NSREF. The stitching of the carbon fibre fabrics therefore did not produce significant differences in the tensile failure strain of the composites. However, removing the stitches from the 76HT fabric type resulted in a statistically significant decrease of the failure strain with a p-value of 0.04%. A second panel of the 76HTSR composite type was produced and tested and showed the same result (see 76HTSR2 in Figure 3 and Table 1).

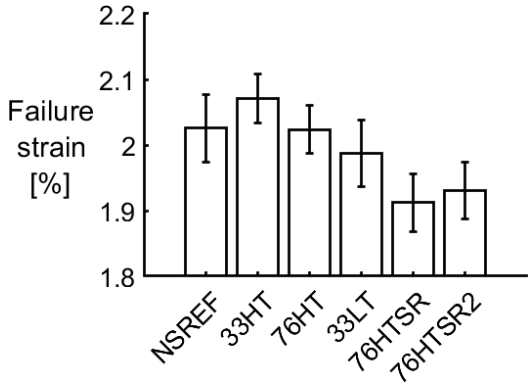

***Figure 3** – Failure strain and respective 95% confidence intervals for the 5 different types of stitched fabrics tested.*

***Table 1** – Number of specimens, failure strain with 95% confidence intervals, and p-values for a two-tailed, heteroscedastic Student's t-test.*

Configuration	# of specimens	Failure strain (%)	p-values					
			NSREF	33HT	76HT	33LT	76HTSR	76HTSR2
NSREF	11	2.03±0.05	-	0.12	0.95	0.25	1.10^{-3}	5.10^{-3}
33HT	10	2.07±0.04	-	-	0.05	8.10^{-3}	8.10^{-6}	3.10^{-5}
76HT	10	2.02±0.04	-	-	-	0.21	4.10^{-4}	2.10^{-3}
33LT	10	1.99±0.05	-	-	-	-	0.02	0.07
76HTSR	10	1.91±0.04	-	-	-	-	-	0.50
76HTSR2	10	1.93±0.04	-	-	-	-	-	-

The expectation was that removing the stitching thread would re-align the fibres and the microstructure and tensile failure strain would become similar to NSREF. Although the fibres did re-align (see section 3.3), its tensile failure strain was lower than all the other

composite types. The main hypothesis is that during the removal of the stitches and/or manufacturing of the composite panel, defects were introduced that caused the reduction of the failure strain. Without the stitching thread, the fabric lost stability in the transverse direction. In the locations where the bundles separated and gaps are formed (see Figure 4), the fibres in the adjacent layer of this fabric are more prone to be near a resin rich region. Near this resin rich region, broken fibres have fewer neighbouring fibres. These neighbouring fibres therefore have to withstand a higher stress concentration and are more likely to fail, reducing the failure strain of the composite [34]. This hypothesis remains to be experimentally proven.

The stitched fabrics also have these gaps due to the passage of the stitching yarn through the fabric, but these are localised at the stitching point. In the fabric with the stitches removed, it is hypothesised that the gap could be constant along the fibre direction (not in field of view of CT scans). The probability of finding a weaker region of the adjacent layer would therefore be higher and could explain the lower failure strain.

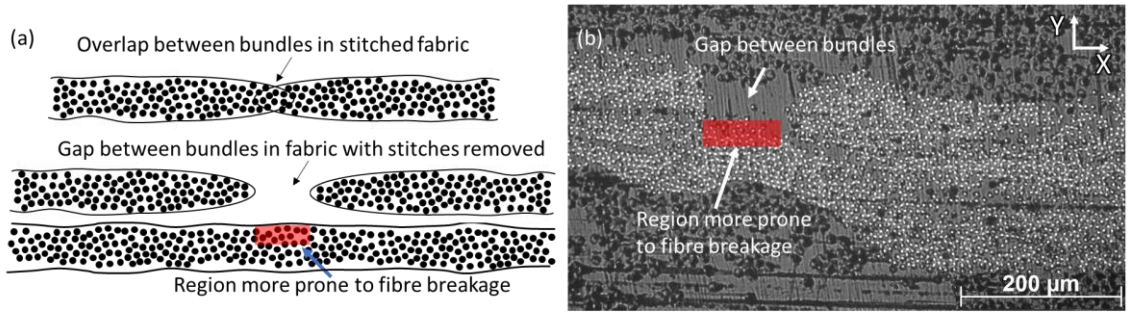

***Figure 4** – Gap between bundles in (a) a schematic showing the region prone to fibre breakage in the adjacent layer and (b) observed in microscopy images of the 76HTSR composite.*

The tensile failure strain was also statistically different between the 33HT and 33LT fabric composites (p-value was 0.8%). It should be noted here that the results in Figure 3 and Table 1 include between 1 and 5 tensile specimens that still failed at the grips for all the composite types. The tensile failure strain tended to be higher as the distance from the fracture location to the grips increased. That tendency was very limited though, leading to the conclusion that the stress concentrations at the grips only had a minor influence in the results. If the failure strain of 33HT and 33LT is analysed using only the specimens that failed away from the grips, the difference is not statistically significant (p-value was 7.2%). This result introduces uncertainty on whether the 33HT and 33LT fabrics lead to composites with a different tensile failure strain. The other conclusions stated so far are not influenced by the distance from the fracture to the grips, as the 33HT, 33LT and 76HT composites are still not statistically different from the NSREF composite.

3.2 Local fibre volume fraction

The spatial variation of local fibre volume fraction was analysed for the 76HT and 33LT fabrics, as these are the two cases that happen in reality and should have the largest difference. As explained in section 2.2.5, the InSegt algorithm could only identify ~80% of all the fibre centres, thus mandating manual identification for the determination of the fibre volume fraction. The two fabrics used for this characterisation were chosen based on the expected distortion of the fibres with the stitches. The 76HT fabric was expected to have the highest distortion due to the high linear density of the yarn and the high tension applied to it. By contrast, the 33LT fabric contained the lowest linear density yarn to

which a lower tension was applied, thus causing the lowest expected distortion. Figure 5 reveals the v_f variation in the X and Z direction for these , with the resin-rich area created by the stitch indicated by the black region.

The 76HT layer containing a stitch shows the features expected for the surroundings of a stitch region: a higher v_f near the centre of the stitch (X=1, Z=0.2) and a decreasing trend when the fibres are farther away from this location. The v_f increases from 55% far from the stitch to a maximum of 72% immediately adjacent to the stitch location. It is also interesting that the v_f distribution is not symmetric relative to the stitch location but there is a larger region with high v_f for X > 1 mm than for X < 1 mm. This seems to be associated with the geometry of the opening created by the stitch (see black region in Figure 5a) where the opening is larger towards X > 0.9 mm. One should therefore be cautious in idealising the stitch as symmetric, even with the chain stitch. The 45º angle of the stitching is likely to be the cause for the asymmetry.

There also seems to be a preferential distribution of the v_f in the 76HT layer that does not contain a stitch. In this layer, there is a high v_f region with an angle of 45º, the same as the orientation of the stitching yarn. In fact, the presence of the stitching yarn between the layers appears to compact the fibres and increase the v_f also in layer 2, adjacent to the layer with a stitch.

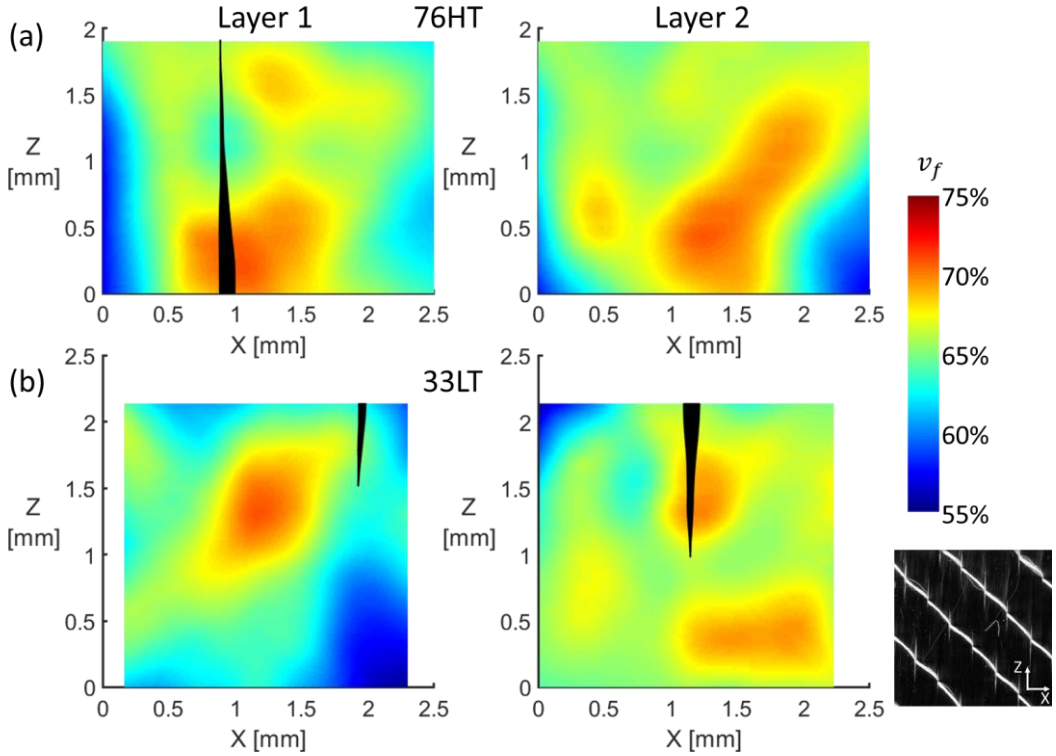

Figure 5 *– Variation of* $\boldsymbol{v_f}$ *as a function of the X and Z position for the (a) 76HT and (b) 33LT fabric. For each fabric type, the* $\boldsymbol{v_f}$ *variation is given for each layer indicated at the top. The black region corresponds to the position of the resin-rich area created by the stitching point opening. The colours indicate the magnitude of the* $\boldsymbol{v_f}$ *as indicated by the colour bar.*

For 33LT, the distribution of v_f does not show a clear pattern as in 76HT. It was expected that the distortion of the fabric would be less pronounced in the 33LT fabric and that

would lead to a smaller influence in the v_f near the stitch. If the closing position of the stitch is compared between 76HT (X = 1 mm, Z = 1.2 mm) with 33LT in layer 2 (X = 1 mm, Z = 1.4 mm), there is a clearly distinctly high v_f in the 33LT fabric whereas there is a low v_f in the 76HT fabric. Still, the high v_f in layer 1 of 33LT in the position near the stitch in layer 2 occurred for the same reason as in 76HT. The fibre distortion therefore seems inconsistent near the stitch across all the fabrics but based on the observations, a higher v_f in the adjacent layer is likely to occur. This region in layer 2 associated to the stitch in layer 1 is not visible in the window of observation because the stitching yarn passes between the layers for X > 2 mm.

The time-consuming nature of this experimental approach limited our analysis to just two specimens. The reported observations are location dependent, and further analysis would help to confirm the reported conclusions.

3.3 Fibre misalignment

The fibre alignment was analysed using one specimen for each fabric type with dimensions of 2-2.5 mm in the X and Z directions. The fibre angle was computed in-plane and out-of-plane. In this section, the main focus will be on the in-plane angle distribution because the fibre distortion due to the stitching is expected to be more significant in this direction. We also expect that the misalignment angle is higher in the in-plane than in the out-of-plane direction. The in-plane fibre angle distribution in the 76HT, 33HT and 33LT fabrics is compared in Figure 6.

The in-plane angle distribution shows that symmetry around the axis of the stitch is possible (see layer 2 in Figure 6c) but it is not as likely as the asymmetry observed in the other layers that contained a stitch. In the 33LT fabric, where one of the stitches produced a symmetric angle distribution, the maximum angle was also lower than in the other layer of the same fabric where the asymmetry was observed. The models that simulate the fibre angle distribution near the stitch [25,26,28] are therefore likely to underestimate the maximum angle due to their symmetry assumption, which is not observed in the real composites.

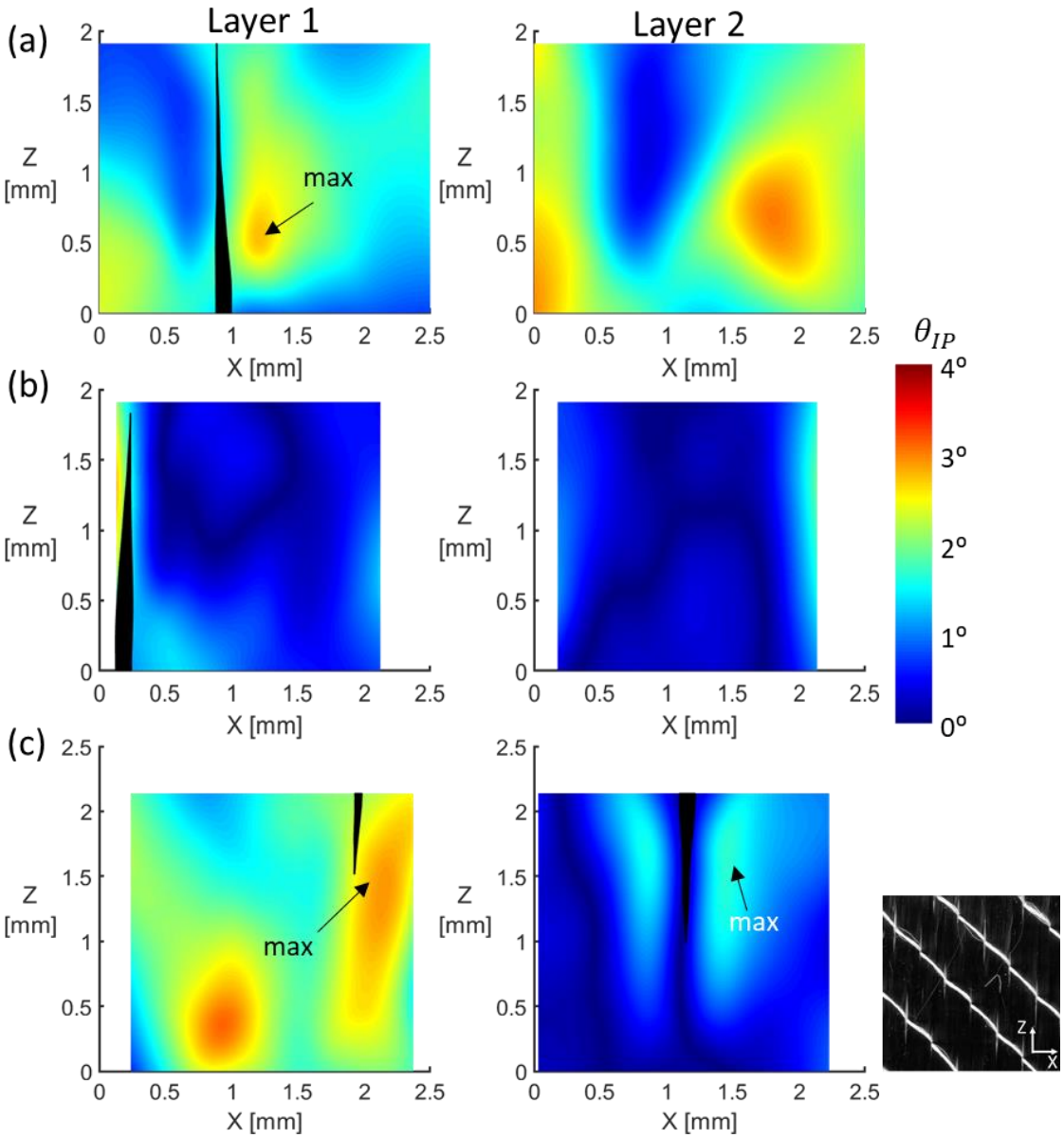

***Figure 6** – In-plane fibre angle spatial distribution in the 2 layers of the (a) 76HT, (b) 33HT and (c) 33LT fabrics. The black region corresponds to the position of the stitching point opening. The colours indicate the magnitude of the $\boldsymbol{\theta_{IP}}$ as indicated by the colour bar.*

The maximum θ_{IP} was not observed in the same Z plane as the centre of the stitch but rather close to the inflection point of the stitch region boundary (see layer 1 in Figure 6a). For the 33HT fabric, the maximum θ_{IP} seems to occur for X = 0 mm and therefore the side of the stitch where the maximum angles occurred was outside of the observation window. The maximum θ_{IP} for the 76HT fabric where the maximum distortion was expected was 3.7º. However, the maximum θ_{IP} observed was in layer 2 of the 76HT fabric where no stitch was present and in the layer 1 of 33LT fabric far from the stitch location. It seems therefore that although the stitching points have an influence on the fibre angle, there are regions far from the stitch locations where θ_{IP} is also high. Overall, there does not seem to be a correlation between the local fibre volume fraction (see Figure 5) and in-plane fibre misalignment.

The non-stitched fabrics such as the NSREF and the 76HTSR fabrics had a lower fibre angle with a maximum of 1.6º compared to the maximum of 3.8º in the stitched fabrics, as shown in Figure 7. In these fabrics, there was no preferential distribution of the θ_{IP}. Two specimens of the 76HTSR fabrics were exceptionally scanned because the one shown in Figure 7b did not show a high fibre misalignment angle or the presence of one of the resin channels hypothesised in section 3.1. In the CT images, the second specimen of 76HTSR (see Figure 7c) appeared to have one of these resin channels or the previous location of a stitch in layer 2 for X = 2.1 mm but this did not produce a high θ_{IP} near this region. In the observed specimens of the 76HTSR fabric, the θ_{IP} was indeed under 2º over the entire observation window, which is a distinctly low value compared to observations of the stitched fabrics. This confirms that the fibre alignment in the 76HTSR fabrics was recovered by the removal of the stitching yarns. It also reinforces the hypothesis that some mechanism(s) other than fibre misalignment caused the decrease in tensile failure strain.

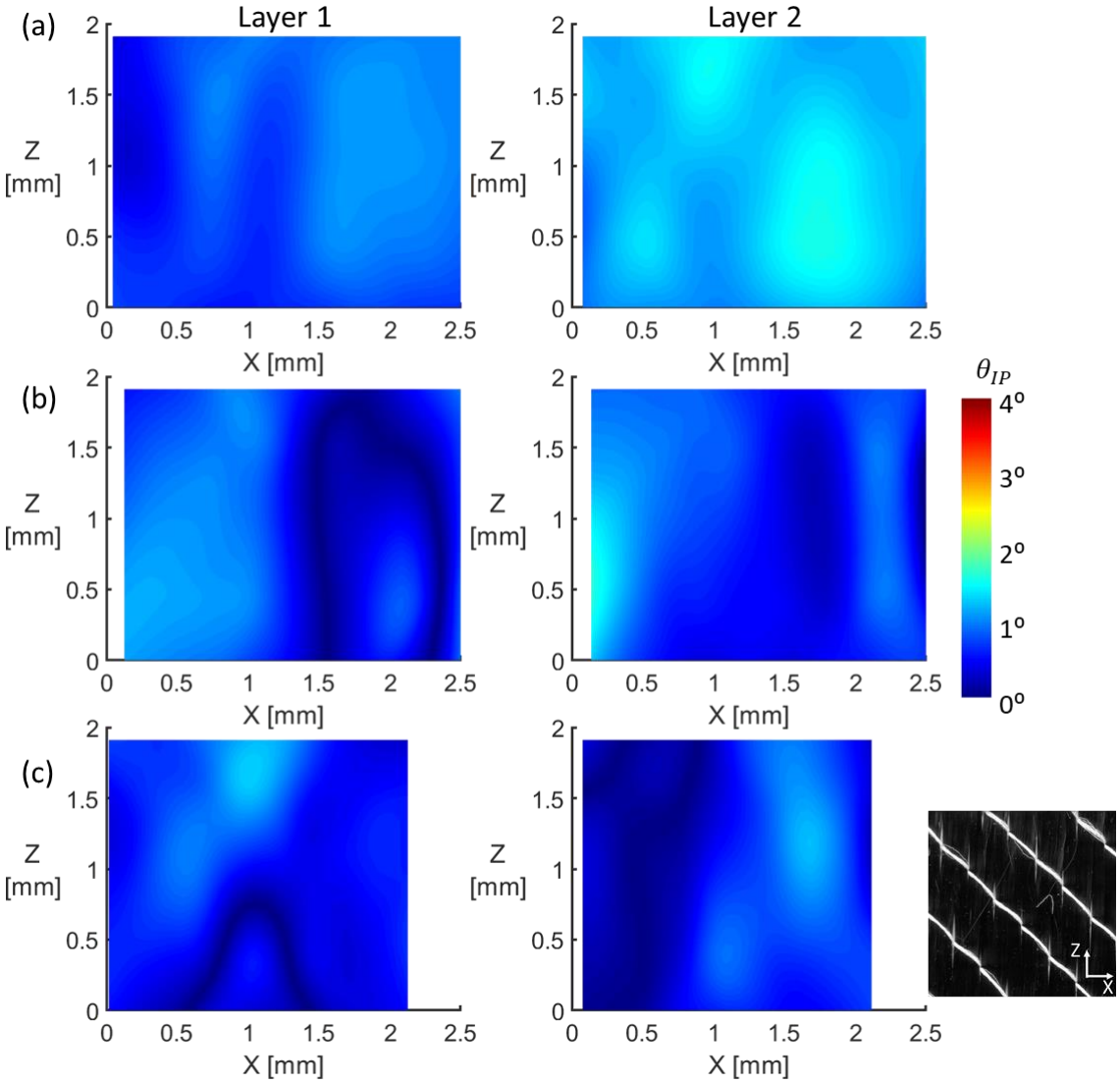

***Figure 7** – In-plane fibre angle spatial distribution in the 2 layers of the (a) NSREF, (b) specimen 1 of 76HTSR and (c) specimen 2 of 76HTSR fabrics. The black region corresponds to the position of the stitching point opening. The colours indicate the magnitude of the $\boldsymbol{\theta_{IP}}$ as indicated by the colour bar.*

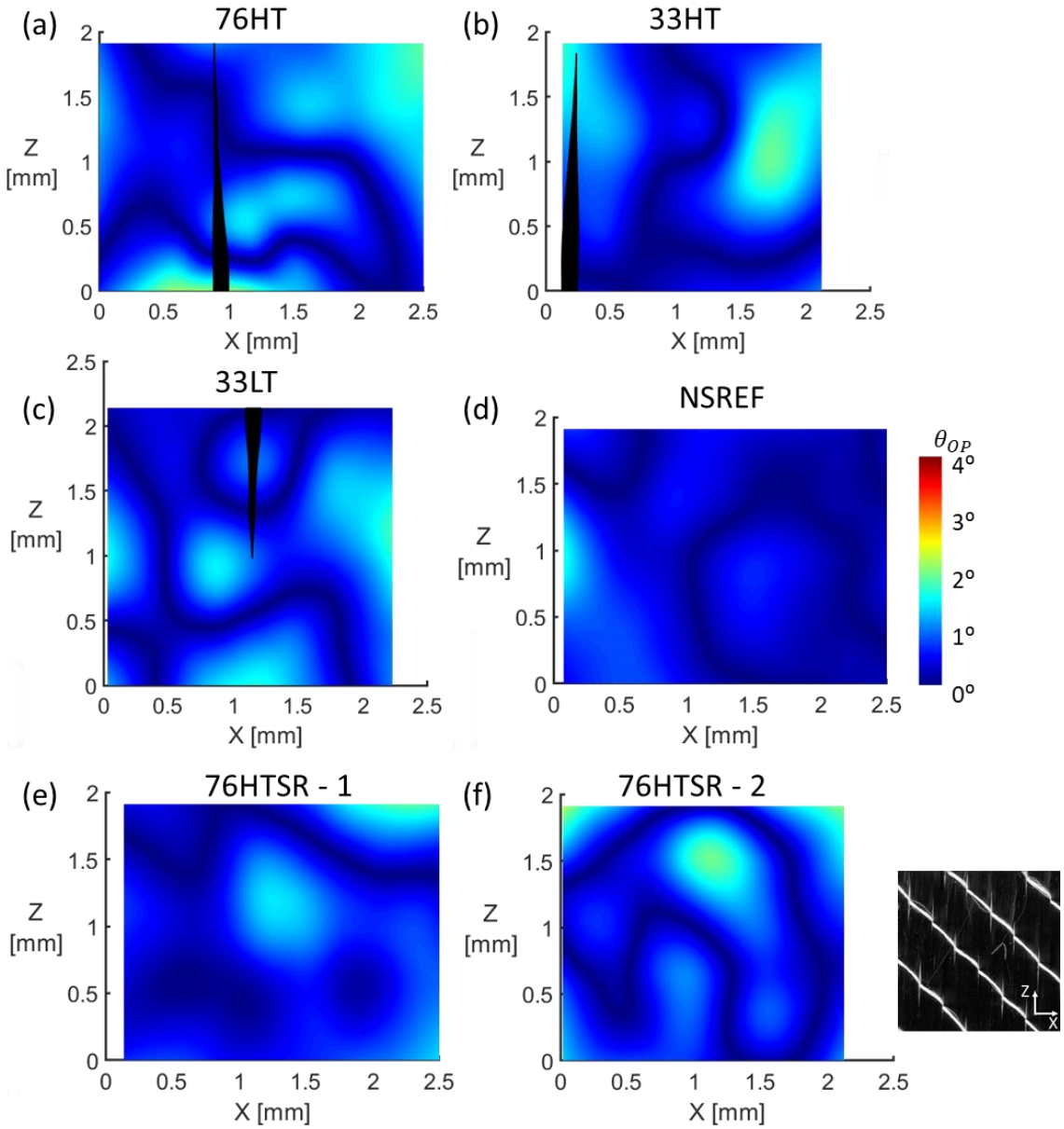

Figure 8 *– Out-of-plane fibre angle spatial distribution in the (a) 76HT (layer 1), (b) 33HT (layer 1), (c) 33LT (layer 2), (d) NSREF (layer 2), (e) specimen 1 of 76HTSR (layer 2) and (f) specimen 2 of 76HTSR (layer 1) fabrics. The black region corresponds to the position of the stitching point opening. The colours indicate the magnitude of the* $\boldsymbol{\theta_{OP}}$ *as indicated by the colour bar.*

The out-of-plane fibre angle, θ_{OP}, was not generally affected by the stitching. The only exception is observed in Figure 8a for the 76HT fabric. As shown in Figure 2a, the stitching yarn is not only between two bundles of the same yarn but also over the bundle in the right side of the image. It is therefore possible that the stitching yarn influences the out-of-plane angle, but this is more likely to happen in fabrics with a high stitching yarn density because it requires more space between the fibre bundles. In general, however, the θ_{OP} was lower than the θ_{IP} in the same fabrics. The final observation is that a network of low θ_{OP} seems to exist in each layer, evidenced by the dark blue regions in Figure 8. These low θ_{OP} are not likely to produce a change in the tensile failure strain of the composite but deserve further investigation to understand whether they are real or just an

artefact of the InSegt algorithm. A smaller voxel size would aid in the fibre identification and could clarify this observation.

The out-of-plane misalignment angles reported here are small compared to Rouf et al. [23]. They used heavier tows (50K instead of 12K), but also do not report any stitching parameters. The fact that we only had 2 UD NCF layers and the addition of UD glass layers without any crimp in them, would also contribute to minimising the out-of-plane misalignment. Nevertheless, it remains very difficult to compare these papers against each other.

4 Conclusions

The tensile failure strain of a UD NCF composite appears unaffected by the presence of stitches in the dry fabrics. The only composite that showed a significantly different tensile failure strain relative to the NSREF composite was the 76HTSR in which the stitching thread was removed manually. The difference in tensile failure strain may be explained by the lower stability of the fabric in the transverse direction that can lead to resin channels that may increase the fibre break rate in the adjacent layer. It would be interesting to compare the tensile failure strain of fabrics with induced resin channels and local fibre distortions.

The fibre volume fraction distribution showed characteristics consistent with the expectation where the 76HT had a high v_f in the plane of the stitch centre. Still, the v_f distribution was not symmetric relative to the stitch region. The stitching yarn is also responsible for an increased v_f in the adjacent layer to the stitching point due to the compaction of the fibres. The 33LT fabric, with a lower yarn tension and linear density did not show the expected characteristics of high v_f nearer to the stitch. Still an increase in v_f due to the compaction of the fibres in the presence of the stitching yarn was observed.

The in-plane fibre angle was affected by the presence of the stitch with the 76HT clearly showing an increased θ_{IP} close to the inflection point of the stitch. The distribution of θ_{IP} was also not symmetric relative to the stitch except in one layer of the 33LT fabric. The non-stitched fabrics as the NSREF and 76HTSR fabrics showed a lower maximum in-plane misalignment angle relative to the stitched fabrics. Even though the presence of the stitches contributed to the increase in fibre angle, there were regions of the stitched fabrics that were seemingly far from stitches and still displayed high θ_{IP} values. The presence of stitches was less important for the out-of-plane angle θ_{OP}. The only case where this was not true, was for the 76HT fabric where the yarn density is higher. The stitching point did not have space between fibre bundles, distorting one of the bundles in the thickness direction.

The results suggest that UD NCFs with fibre distortions can be used for structural applications without fearing the degradation of tensile failure strain of the composite.

5 Acknowledgments

The research leading to these results has been done within the framework of the FiBreMoD project and has received funding from the European Union's Horizon 2020 research and innovation programme under the Marie Skłodowska-Curie grant agreement

No 722626. SVL holds Toray Chair for Composite Materials, the support of which is acknowledged. The authors would also like to thank Jeroen Soete for the support in the acquisition of the computed tomography scans. The FWO large infrastructure I013518N project is acknowledged for their financial support of the X-ray infrastructure and the KU Leuven XCT Core Facility is acknowledged for the 3D image acquisition and post-processing tools (https://xct.kuleuven.be/).

6 References

[1] Rosen BW. *Tensile failure of fibrous composites*. AIAA Journal. 1964;2(11):1985-1991.
[2] Heß H, Himmel N. *Structurally stitched NCF CFRP laminates. Part 2: Finite element unit cell based prediction of in-plane strength*. Composites Science and Technology. 2011;71(5):569-585.
[3] Heß H, Himmel N. *Structurally stitched NCF CFRP laminates. Part 1: Experimental characterization of in-plane and out-of-plane properties*. Composites Science and Technology. 2011;71(5):549-568.
[4] Koissin V, Kustermans J, Lomov SV, Verpoest I, Van Den Broucke B, Witzel V. *Structurally stitched NCF preforms: Quasi-static response*. Composites Science and Technology. 2009;69(15):2701-2710.
[5] Truong TC, Vettori M, Lomov SV, Verpoest I. *Carbon composites based on multi-axial multi-ply stitched preforms. Part 4. Mechanical properties of composites and damage observation*. Composites Part A: Applied Science and Manufacturing. 2005;36(9):1207-1221.
[6] Rimmel O, May D, Mitschang P. *Impact of stitching on permeability and mechanical properties of preforms manufactured by dry fiber placement*. Polymer Composites. 2019;40(4):1631-1642.
[7] Mouritz AP, Leong KH, Herszberg I. *A review of the effect of stitching on the in-plane mechanical properties of fibre-reinforced polymer composites*. Composites Part A: Applied Science and Manufacturing. 1997;28(12):979-991.
[8] Kang TJ, Lee SH. *Effect of Stitching on the Mechanical and Impact Properties of Woven Laminate Composite*. Journal of Composite Materials. 1994;28(16):1574-1587.
[9] Dransfield K, Baillie C, Mai Y, *The Mode II delamination fracture toughness of stitched CFRPs*, 2nd Pacific International Conference on Aerospace and Technology conference, Sixth Australian Aeronautical Conference, 1995.
[10] Pelstring R, Mandan R, *Stitching to improve damage tolerance of composites*, 34th International SAMPE symposium, Reno, USA, 1989.
[11] Palmer RJ, Dow MB, Smith DL, *Development of stitching reinforcement for transport wing panels*, First NASA Advanced Composites Technology Conference Part 2, Seattle, USA, 1990.
[12] Lomov SV. *Non-crimp fabric composites*. 1st ed. Cambridge: Woodhead Publishing; 2011.
[13] Bibo GA, Hogg PJ, Kemp M. *Mechanical characterisation of glass- and carbon-fibre-reinforced composites made with non-crimp fabrics*. Composites Science and Technology. 1997;57(9):1221-1241.
[14] Asp LE, Edgren F, Sjögren A, *Effects of stitch pattern on the mechanical properties of non-crimp fabric composites*, 11th European Conference on Composite Materials, Rhodes, Greece, 2004.

[15] Li L, Zhao Y, Zhang L, Li W, *Evaluating deformability of non-crimp fabric and mechanical performance of non-crimp fabric composites*, 19th International Conference on Composite Materials, Montréal, Canada, 2013.
[16] Mikhaluk DS, Truong TC, Borovkov AI, Lomov SV, Verpoest I. *Experimental observations and finite element modelling of damage initiation and evolution in carbon/epoxy non-crimp fabric composites*. Engineering Fracture Mechanics. 2008;75(9):2751-2766.
[17] Malgioglio F, Pimenta S, Matveeva A, Farkas L, Desmet W, Lomov SV, et al. *Microscale material variability and its effect on longitudinal tensile failure of unidirectional carbon fibre composites*. Composite Structures. 2021;261:113300.
[18] Swolfs Y. *Hybridisation of Self-reinforced Composites: Modelling and Verifying a Novel Hybrid Concept* PhD thesis. KU Leuven, Department of Materials Engineering, 2015.
[19] Herszberg I, Bannister MK, *Tensile properties of thin stitched carbon/epoxy composites*, 5th Australia Aeronautical Conference, Melbourne, Australia, 1993.
[20] Sinclair JH, Chamis CC. *Fracture modes in off-axis fiber composites*. Polymer Composites. 1981;2(1):45-52.
[21] Reeder JR. *Stitching vs. a Toughened Matrix: Compression Strength Effects*. Journal of Composite Materials. 1995;29(18):2464-2487.
[22] Chang P, Mouritz AP, Cox BN. *Properties and failure mechanisms of z-pinned laminates in monotonic and cyclic tension*. Composites Part A: Applied Science and Manufacturing. 2006;37(10):1501-1513.
[23] Rouf K, Worswick MJ, Montesano J. *A multiscale framework for predicting the mechanical properties of unidirectional non-crimp fabric composites with manufacturing induced defects*. Journal of Composite Materials. 2020;55(6):741-757.
[24] González A, Graciani E, París F. *Prediction of in-plane stiffness properties of non-crimp fabric laminates by means of 3D finite element analysis*. Composites Science and Technology. 2008;68(1):121-131.
[25] Wei Y, Zhang J. *Characterization of microstructure in stitched unidirectional composite laminates*. Composites Part A: Applied Science and Manufacturing. 2008;39(5):815-824.
[26] Yavari V, Kadivar MH. *Fiber Volume Fraction around Stitch in NCF Composites*. Procedia Engineering. 2011;14:3191-3198.
[27] Auenhammer RM, Mikkelsen LP, Asp LE, Blinzler BJ. *Automated X-ray computer tomography segmentation method for finite element analysis of non-crimp fabric reinforced composites*. Composite Structures. 2021;256:113136.
[28] Truong TC, Ivanov DS, Klimshin DV, Lomov SV, Verpoest I. *Carbon composites based on multi-axial multi-ply stitched preforms. Part 7: Mechanical properties and damage observations in composites with sheared reinforcement*. Composites Part A: Applied Science and Manufacturing. 2008;39(9):1380-1393.
[29] Czél G, Jalalvand M, Wisnom MR. *Hybrid specimens eliminating stress concentrations in tensile and compressive testing of unidirectional composites*. Composites Part A: Applied Science and Manufacturing. 2016;91:436-447.
[30] Wisnom MR, Czel G, Swolfs Y, Jalalvand M, Gorbatikh L, Verpoest I. *Hybrid effects in thin ply carbon/glass unidirectional laminates: accurate experimental determination and prediction*. Composites Part A: Applied Science and Manufacturing. 2016;88:131-139.

[31] *ASTM D3039-14 Standard Test Method for Tensile Properties of Polymer Matrix Composite Materials*, Philadelphia, USA, ASTM, 2014.
[32] Emerson MJ, Jespersen KM, Dahl AB, Conradsen K, Mikkelsen LP. *Individual fibre segmentation from 3D X-ray computed tomography for characterising the fibre orientation in unidirectional composite materials*. Composites Part A: Applied Science and Manufacturing. 2017;97:83-92.
[33] Dahl VA, Trinderup CH, Emerson MJ, Dahl AB. *Content-based Propagation of User Markings for Interactive Segmentation of Patterned Images*. Proc Comput Vis Microsc Im Anal (CVMI) workshop, IEEE. 2020;35.
[34] Swolfs Y, Verpoest I, Gorbatikh L. *Issues in strength models for unidirectional fibre-reinforced composites related to Weibull distributions, fibre packings and boundary effects*. Composites Science and Technology. 2015;114:42-49.